

Endogenous microRNA Triggered Enzyme-free DNA Logic Self-assembly for Amplified Bioimaging and Enhanced Gene Therapy via in Situ Generation of siRNAs

Qinghua Jiang

The Affiliated Hospital of Qingdao University

Shuzhen Yue

Qingdao University

Kaixin Yu

Qingdao University

Tian Tian

The Affiliated Hospital of Qingdao University

Jian Zhang

Qingdao University

Huijun Chu

The Affiliated Hospital of Qingdao University

Zhumei Cui

The Affiliated Hospital of Qingdao University

Sai Bi (✉ bisai11@126.com)

Qingdao University

Research Article

Keywords: DNA nanotechnology, miRNA, siRNA, gene therapy, cervical carcinoma

Posted Date: August 2nd, 2021

DOI: <https://doi.org/10.21203/rs.3.rs-729136/v1>

License:  This work is licensed under a Creative Commons Attribution 4.0 International License.

[Read Full License](#)

Abstract

Background

Small interfering RNA (siRNA) has emerged as a kind of promising therapeutic agents for cancer therapy. However, the off-target effect and degradation are the main challenges for siRNAs delivery. Herein, an enzyme-free DNA amplification strategy initiated by a specific endogenous microRNA has been developed for *in situ* generation of siRNAs with enhanced gene therapy effect on cervical carcinoma.

Methods

This strategy contains three DNA hairpins (H1, H2/PS and H3) which can be triggered by microRNA-21 (miR-21) for self-assembly of DNA nanowheels (DNWs). Notably, this system is consistent with the operation of a DNA logic circuitry containing cascaded “AND” gates with feedback mechanism. Accordingly, a versatile biosensing and bioimaging platform is fabricated for sensitive and specific analysis of miR-21 in HeLa cells via fluorescence resonance energy transfer (FRET). Meanwhile, since the vascular endothelial growth factor (VEGF) antisense and sense sequences are encoded in hairpin reactants, the performance of this DNA circuit leads to *in situ* assembly of VEGF siRNAs in DNWs, which can be specifically recognized and cleaved by Dicer for gene therapy of cervical carcinoma.

Results

The proposed isothermal amplification approach exhibits high sensitivity for miR-21 with a detection limit of 0.25 pM and indicates excellent specificity to discriminate target miR-21 from the single-base mismatched sequence. Furthermore, this strategy achieves accurate and sensitive imaging analysis of the expression and distribution of miR-21 in different living cells. To note, compared to naked siRNAs alone, *in situ* siRNA generation shows a significantly enhanced gene silencing and anti-tumor effect due to the high reaction efficiency of DNA circuit and improved delivery stability of siRNAs.

Conclusion

The endogenous miRNA-activated DNA circuit provides an exciting opportunity to construct a general nanoplatform for precise cancer diagnosis and efficient gene therapy, which has an important significance in clinical translation.

Introduction

SiRNAs are short double-stranded RNA molecules with 20-25 base pairs, which have acted as efficient biotherapeutic agents to treat many diseases by inducing post-transcription gene silencing [1-6]. However, the delivery of naked siRNAs by lipids, polymers and nanomaterials often shows the limitations of non-specific absorption, low efficiency of cellular uptake and potential cytotoxicity, which thus hamper their clinical applications [7-10]. Recently, DNA nanotechnology has rapidly developed to construct a variety of nanocarriers for siRNA delivery based on the good biocompatibility and programmability, such as DNA

origami [11], DNA nanohydrogels [12], and so on. For these strategies, the integration of siRNAs into DNA nanostructures mainly relies on the hybridization or chemical modification, thus, the unavoidable leakage and degradation, as well as the limited payload capacity may diminish the gene therapy efficiency [13-15]. As an alternative method, *in situ* generation of siRNAs can significantly enhance the specificity and delivery stability, which thus provides a robust and powerful strategy for cancer therapy [16, 17].

It has been found the aberrant expression of miRNA is closely related to many cancers, such as lung carcinoma [18], breast cancer [19], pancreatic cancer [20], and so on. Therefore, it is of far reaching importance to detect miRNA for early cancer diagnosis [21, 22]. At present, northern blotting is commonly used for miRNA detection [23, 24]. Also, some enzyme-mediated nucleic acid signal amplification methods, including polymerase chain reaction (PCR) [25] and rolling circle amplification (RCA) [26], have been widely used for quantification of miRNA [27]. However, the drawbacks such as harsh reaction conditions, low sensitivity, and the involvement of exotic enzymes make these methods unsuitable for further applications in living cells [28, 29]. Recently, a variety of enzyme-free DNA nanotechnology-based methods, especially DNA strand displacement reactions, have been developed for *in situ* imaging and quantification of miRNA in living cells due to the advantages of simple operation and isothermal features [30-35]. More importantly, as an important biomarker of cancers, the combination of biosensing and bioimaging of miRNA with therapy modalities is of great significance to monitor disease progression in response to treatment, which may offer innovative platforms for theranostics and precision medicine [36-40].

Herein, a miRNA-responsive AND-gate cascaded DNA logic circuit with target feedback function has been developed, which has achieved enzyme-free isothermal amplification of miR-21 in living cells and *in situ* generation of VEGF siRNA for enhanced gene therapy of cervical carcinoma. This system contains three kinds of DNA hairpins (H1, H2/PS and H3), in which miR-21 triggers the catalytic hairpin assembly, resulting in the sensitive and selective biosensing and bioimaging of miR-21 in HeLa cells along with the formation of DNA nanowheels (DNWs). As a result, numerous VEGF siRNAs are *in situ* generated in DNWs, achieving the efficient inhibition of VEGF mRNA and protein expression for gene therapy of cervical carcinoma. Compared to the traditional methods for siRNA delivery, our proposed strategy with *in situ* generation of siRNA in living cells presents a significantly improved delivery efficiency and stability, which thus offers a robust and powerful approach for specific gene silencing and cancer therapy.

Materials And Methods

Materials and reagents

All oligonucleotides used in this work were synthesized and purified by Sangon Biotechnology Co., Ltd. (Shanghai, China), and their sequences are listed in Additional files 1: Table S1. Fetal bovine serum (FBS) and Dulbecco's modified Eagle's (DMEM) medium were obtained from Biological Industries (Israel) and HyClone (USA), respectively. Lipofectamine 3000 was ordered from ThermoFisher scientific (USA). Annexin V-FITC apoptosis detection kit was purchased from CoWin Biosciences (Beijing, China). Hoechst

33342 solution, 4S Red Plus Nucleic Acid Stain and N, N, N', N'-tetramethyl ethylenediamine (TEMED) were ordered from Sangon Biotechnology Co., Ltd. (Shanghai, China). All the reagents were of analytical grade and used without further purification.

Preparation of DNA hairpins

The stock solutions of oligonucleotides (100 μ M) were prepared using deionized ultrapure water, which were further diluted to 10 μ M using TE buffer (10 mM Tris-HCl, 1 mM EDTA-2Na, 12.5 mM MgCl₂, pH 7.4). To obtain the desirable secondary structures, the DNA hairpin strands (H1, H2 and H3) were respectively annealed in TE buffer by heating to 95 °C for 10 min, followed by cooling to 25 °C with a rate of 0.1 °C/s and standing at 25 °C for 4 h before each use. Further, H2 was incubated with equal amount of protect strand (PS) at 37 °C for 2 h to form the H2/PS hybrid.

Native polyacrylamide gel electrophoresis

The 8% polyacrylamide gel (PAGE) was prepared according to the previous study [32], followed by adding 10 μ L of each sample and 2 μ L of 10× loading buffer. Then, the native PAGE was running at 170 V for 5 min and 110 V for 35 min in 1× TAE buffer (10 mM Tris, 1 M glacial acetic acid, 1 mM EDTA-2Na, 12.5 mM MgCl₂, pH 8). Finally, the resulting gel was stained with 4S Red Plus solution for about 30 min and recorded by Tanon 2500R gel imaging system (Shanghai, China).

Atomic force microscopy imaging

A 10 μ L of each sample was deposited onto the freshly cleaved mica for 30 min. Then, the mica surfaces were washed using deionized ultrapure water for three times, followed by drying at room temperature. Finally, the samples were scanned by Being Nano-Instruments CSPM-4000 system (Guangzhou, China) under the tapping mode. The obtained images were analyzed using CSPM Console software.

Fluorescence measurements

A 2 μ L of miR-21 with different concentrations was added to the mixture of H1, H2/PS and H3 (10 μ L and 200 nM for each species), respectively. The real-time fluorescence was monitored on a LineGene 9600 Real-Time detection system (Hangzhou, China) at an interval of 30 s ($\lambda_{\text{ex}} = 470$ nm and $\lambda_{\text{em}} = 525$ nm) for 4 h. The reaction temperature was set at 37 °C. The corresponding fluorescence spectra at 4 h were recorded on a F-7000 fluorescence spectrophotometer (Hitachi, Japan).

Stability assays

The naked VEGF siRNA (100 nM) and VEGF siRNA formed in DNWs (100 nM) was incubated in 100 μ L of HeLa cell lysate solution for 1 h, 2 h, 3 h and 4 h, respectively. Subsequently, 15% PAGE was performed to study the stability [36].

Cell culture

The HeLa cells (human cervix carcinoma cell), HepG2 cells (human liver cancer line) and L-02 cells (human normal liver cell line) were purchased from Shanghai Institutes for Biological Sciences (SIBS) (Shanghai, China) and cultured in DMEM supplemented with 10% FBS, streptomycin (100 µg/mL) and penicillin-streptomycin (100 µg/mL) at 37 °C under 5% CO₂ humid atmosphere. The cells were counted using a cell counting chamber (ThermoFisher scientific, USA) before each assay.

Confocal laser scanning microscopy imaging

The HeLa cells, HepG2 cells and L-02 cells were seeded in 48-well plate (3×10^4 cells/well, 500 µL) and cultured in DMEM medium for 12 h, respectively. According to the manufacturer instructions, HeLa cells were transfected with DNA circuit, C-circuit and R-circuit, respectively, in which the DNA circuit contains H1, H2/PS and H3 to generate VEGF siRNA triggered by miR-21, C-circuit contains H1-C, H2-C and H3-C to generate negative control siRNA triggered by miR-21, and R-circuit contains random DNA (H1-R, H2-R and H3-R) that is not responsive to miR-21. In addition, the antisense miR-21 pretreated HeLa cells were transfected with DNA circuit. The final concentration of each DNA hairpin was 200 nM. After incubation for 4 h at 37 °C, the cells were washed with PBS for three times, and the fluorescence images were recorded on a Nikon Confocal Microscope A1 (Nikon, Japan) ($\lambda_{\text{ex}} = 488$ nm and $\lambda_{\text{em}} = 520 \pm 20$ nm). For nuclear localization imaging, the HeLa cells were incubated with DNA circuit (200 nM for each DNA hairpin) for 4 h, followed by staining with Hoechst 33342 solution (5 µg/mL) for 30 min. After washing with 1× PBS for three times, the fluorescence images were recorded with an excitation wavelength of 405 nm and an emission wavelength of (475 ± 25) nm using a Nikon Confocal Microscope A1

Flow cytometry

The HeLa cells, HepG2 cells and L-02 cells were seeded in 6-well plates (5×10^5 cells /well) for 12 h and then transfected with DNA circuit for 4 h, respectively. Then, the cells were washed three times with 1× PBS and detached from the plate by trypsin. Finally, the flow cytometry assays were performed on a CytoFLEX system (Beckman Coulter, US) under the excitation of 488 nm.

Quantitative real-time PCR

The HeLa cells and HepG2 cells were seeded in 6-well plates (5×10^5 cells /well) for 12 h and then transfected with different samples (naked siRNA, DNA circuit, C-circuit, R-circuit and Lipo for HeLa cells; C-circuit, R-circuit and DNA circuit for HepG2 cells) for 48 h at 37 °C, respectively. The final concentration of each DNA hairpin was 200 nM. The total RNAs were extracted from the transfected cells using Trizol reagent (Invitrogen, USA). Then, the cDNA was generated using PrimeScriptRT reagent kit (Takara, Japan). Finally, the qRT-PCR analysis was performed using TB Green^R Premix Ex TaqTM II (TaKaRa, Japan) according to the manufacturer instructions. The PCR primer sequences are listed in Additional files 1: Table S1. The operation conditions of PCR were as follows: an initial step (95 °C for 30 s), followed by 40 cycles (95 °C for 5 s and 60 °C for 30 s). The data were analyzed by normalizing to the expression of GAPDH and using the $2^{-\Delta\Delta CT}$ method. The process of RNA extraction was performed on ice.

Western blot assay

The protein expression of cells was examined using western blot. In brief, the HeLa cells and HepG2 cells were seeded in 6-well plates (5×10^5 cells/well) for 12 h and then transfected with different samples (PBS, naked siRNA, DNA circuit, C-circuit and R-circuit for HeLa cells; PBS, naked siRNA and DNA circuit for HepG2 cells) for 48 h at 37 °C, respectively. The final concentration of each DNA hairpin was 200 nM. Then, the cells were lysed in RIPA (Radio Immunoprecipitation Assay) lysis buffer for 30 min on ice and then scraped immediately. The extracted solution was transferred to an EP tube and centrifuged at 4 °C for 15 min (12000 r/min). The concentration of the total protein was measured using a BCA protein assay kit (CoWin Biosciences, Beijing, China). A 25 µg total protein of each sample were loaded on 10% sodium dodecyl sulfate-polyacrylamide gel electrophoresis (SDS-PAGE) and electro-transferred to polyvinylidene fluoride (PVDF) membrane. After being blocked with PBS buffer containing 5% nonfat dry milk for 2 h, the membranes were incubated with the rabbit anti-VEGFA polyclonal antibody (1:1000 dilution) (Absin Bioscience Inc, Shanghai, China) and β-actin (Santa Cruz Biotechnology, USA) overnight at 4 °C, followed by incubation with goat anti-rabbit IgG-HRP secondary antibody (Absin Bioscience Inc, Shanghai, China) (1:5000 dilution) for another 1 h at room temperature. The protein bands were visualized with a Sparkjade ECL super (Sparkjade Biotechnology, Jinan, China) using Vilber Fusion FX7 Spectra (France).

Cell apoptosis experiments

The HeLa cells and HepG2 cells were seeded in 6-well plates (5×10^5 cells/well) for 12 h and then transfected with different samples (naked siRNA, DNA circuit, C-circuit, R-circuit, and Lipo for HeLa cells; C-circuit, R-circuit and DNA circuit for HepG2 cells) for 48 h at 37 °C, respectively. The final concentration of each DNA hairpin was 200 nM. After washing three times with 1× PBS, the collected cells were stained using Annexin V-FITC/PI Apoptosis Detection Kit according to the manufacturer instructions. Finally, the fluorescence signals of cells were analyzed using Cytomics FC 500 (Beckman, USA).

CCK-8 assay

The HeLa Cells and HepG2 cells were seeded in 96-well plates (5×10^3 cells/well) for 12 h and then transfected with different concentrations of DNA hairpins (50 nM, 100 nM, 150 nM and 200 nM) for 48 h, respectively. After washing twice with PBS, 100 µL of 10% CCK-8 solution (10 µL of CCK-8 reagent and 90 µL of DMEM without FBS) was added into each well and incubated with cells for 30 min. Then, the optical density (OD) at 450 nm was measured using a microplate reader (TECAN Safire 2, Switzerland). The relative cell viability (%) was calculated by $(A_{\text{test}} - A_{\text{blank}})/(A_{\text{control}} - A_{\text{blank}}) \times 100\%$, in which A_{test} , A_{blank} and A_{control} represent the OD₄₅₀ of experimental group, blank group and control group, respectively. In addition, to demonstrate the therapeutic efficiency of *in situ* generated VEGF siRNA, the HeLa cells and HepG2 cells were transfected with different samples (naked siRNA, DNA circuit, C-circuit, R-circuit and Lipo for HeLa cells; C-circuit, R-circuit and DNA circuit for HepG2 cells), respectively, followed by determining the relative cell viability using the above methods.

***In Vivo* antitumor efficacy**

All animal experiments were carried out in agreement with the Institutional Animal Care and Use Committee. The female BALB/c nude mice (5-6 weeks) were acquired from Beijing Vital River Laboratory Animal Technology Co., Ltd (Beijing, China) and randomly divided into five groups with four mice per group. The tumor xenograft models were developed by subcutaneous inoculation with 6×10^6 HeLa cells suspended in 100 μL of PBS. When the tumor volumes grew to 75 mm^3 , the groups were intratumorally injected with 50 μL of PBS, naked siRNA, DNA circuit, C-circuit and R-circuit every two days for eight treatments, respectively (the equivalent siRNA dose for each mouse is 0.25 mg/kg). Meanwhile, the bodyweight and tumor growth were monitored during therapy. The tumor volumes were calculated using the formula of $V = (L \times W^2)/2$, where L and W represent the length and width of tumor, respectively. At the end of the experiment, the mice were sacrificed. In addition, the pathological changes of tumors were analyzed using hematoxylin and eosin (H&E) staining assay and terminal deoxynucleotidyl transferase-mediated dUTP nick-end labeling (TUNEL) staining. To further study the biocompatibility of the proposed DNA circuit *in vivo*, the H&E assay was performed to analyze the pathological changes of major organs including heart, liver, spleen, kidney and lung from mice in different groups. The images were obtained with Pannoramic MIDI (3D HISTECH Ltd., Hungary).

Statistical analysis

The data was expressed as mean \pm standard deviations. We used one-way analysis of variance (ANOVA) to analyze the statistical difference (* means $P \leq 0.05$, ** means $P \leq 0.01$, and *** means $P \leq 0.001$).

Results And Discussion

Principle of miRNA activated enzyme-free DNA circuit

The principle of miRNA activated enzyme-free DNA circuit for *in situ* generation of siRNA for gene therapy is illustrated in Scheme 1. In this study, miR-21 which is closely related to the onset, progression, and prognosis of many cancers is chosen as the model target. As shown in Scheme 1A, three kinds of DNA hairpins (H1, H2 and H3) and a PS are rationally designed, in which H1 is served as the recognition probe for miR-21, while VEGF antisense and sense sequences are incorporated into H2 and H3, respectively. To protect the antisense sequence of VEGF-siRNA, PS hybridizes with H2 to form the H2/PS hybrid. To facilitate FRET, fluorophore FAM and quencher BHQ1 are labeled at 3' and 5' ends of H3, respectively. In the absence of miR-21, H1, H2/PS and H3 can metastably coexist, and no fluorescence signal is observed due to the proximity of FAM and BHQ1 in H3. Upon the introduction of miR-21, it simultaneously serves as the initiator (I) and catalyst to activate the operation of DNA circuit via catalytic hairpin assembly based on strand displacement reaction, resulting in the formation of “DNWs” along with the recovery of fluorescence signal. In brief, miR-21 first binds to the toehold domain 1 of H1 and undergoes a DNA toehold-mediated strand displacement reaction to open H1. Then, the newly exposed single-stranded region of H1 hybridizes with domain 3 of H2/PS, replacing PS strands to form the I/H1/H2 hybrid.

Subsequently, H3 hybridizes with I/H1/H2 hybrid, opening the hairpin structure of H3. Analogously, the unfolded region of H3 again opens H1 to trigger the cascaded self-assembly reactions among DNA hairpins until miR-21 is displaced, leading to the formation of “DNWs”. Meanwhile, the released miR-21 is reusable in another reaction cycle to make the self-assembly process operate in a catalytic fashion. Interestingly, the behavior of catalytic hairpin assembly is consistent with the operation of a DNA logic circuitry which consists of cascades of AND gates. Briefly, miR-21 hybridizes with H1 to activate the first AND gate (AND 1), in which miR-21 and H1 act as the inputs, while the I-H1 hybrid as the output. Then, the resulting output and H2/PS work as the inputs to trigger the operation of the second AND gate (AND 2), resulting in the generation of I/H1/H2 output. Subsequently, the third AND gate (AND 3) is activated by H3 which hybridizes with I/H1/H2 to form the hybrid I/H1/H2/H3. Since the exposed sequence of H3 is identical with miR-21, the formed output I/H1/H2/H3 can again hybridizes with H1 to initiate the following cascaded AND gates until miR-21 is replaced, resulting in the formation of “DNWs” as the output. The released miR-21 as a catalyst unit facilitate the feedback mechanism for isothermal signal amplification. In particular, the VEGF antisense and sense sequences are incorporated into H2 and H3, which allows the *in situ* generation of numerous VEGF siRNAs in “DNWs”. By means of endogenous enzyme (Dicer) processing, VEGF siRNA can be specifically cleaved to suppress the expression of corresponding mRNA and protein, achieving efficient gene therapy of cervical carcinoma (Scheme 1B).

Feasibility of enzyme-free DNA circuit

The reaction pathways of the proposed enzyme-free DNA circuit triggered by miR-21 are first verified using PAGE (Fig. 1A). The slow mobility of H2/PS hybrid (lane 4) confirms its successful formation compared with H2 (lane 3). When H1 is mixed with the equal amount of miR-21, a new band corresponding to I/H1 is generated because miR-21 opens the hairpin structure of H1 through toehold-mediated strand displacement reaction (lane 6). Upon the introduction of H2/PS, a new band represented the I/H1/H2 hybrid is produced (lane 7). After addition of H3 into I/H1/H2, the reaction products show two bands with much low and high mobility, respectively, demonstrating the generation of DNA assembly along with the release of miR-21 for recycling (lane 8). In contrast, in the absence of miR-21, no new band is observed, indicating the excellent specificity of the enzyme-free DNA circuit in response to miR-21 and there is no leakage without target (lane 9). The feasibility of this miRNA-responsive DNA circuit was further characterized by AFM (Fig. 1B). In the absence of miR-21, only some small spots are observed, indicating no assembled product is yielded. In contrast, a large amount of monodispersed spherical-like structures with an average height of 18 nm are appeared upon the introduction of 0.1× miR-21 into the system. This phenomenon is well agreed with the results of native PAGE, which further confirm the performance of DNA circuit as expected.

In vitro detection of miR-21

First, the kinetics of the proposed DNA circuit was studied by labeling fluorophore (FAM) and quencher (BHQ1) at 3' and 5' ends of H3, respectively. Upon the introduction of miR-21 with different concentrations, the real-time fluorescence is monitored with a 30 s interval for 4 h (Fig. 2A). In the

absence of miR-21, the fluorescence of FAM is quenched by BHQ1. In contrast, the fluorescence intensity gradually increases with increasing the concentration of miR-21, which demonstrates the high target dependence of DNA circuit. Then, miR-21 was quantitatively detected by measuring the fluorescence spectra after treated with different concentrations of miR-21 for 4 h. As shown in Fig. 2B, the fluorescence intensities are gradually enhanced with the increase of miR-21 ranging from 1 pM to 100 nM. A good linear relationship is presented between miR-21 concentration and fluorescence intensity at 520 nm with a detection limit of 0.25 pM (3σ) (Fig. 2C).

Further, to verify the specificity of the proposed enzyme-free DNA circuit, different targets, including single-base mismatched miR-21 (1mis miR-21), three-base mismatched miR-21 (3mis miR-21), miR-145 and miR-21 are analyzed, respectively (Fig. 2D). As expected, in comparison to the control group without any target, only miR-21 induces an intensified fluorescence. When the recognition domain in H1 is replaced with the non-specific sequence for miR-21 (the sequences of H2 and H3 are changed accordingly) (R-circuit), no enhanced fluorescence is observed, which further proves that the operation of this DNA circuit is highly dependent on the specific Watson-Crick base pairing. Given the high sensitivity and specificity, our proposed enzyme-free DNA circuit in the response to miR-21 has a promising prospect for further application in complex cellular environment.

MiR-21 imaging in living cells

It has been reported that miR-21 is overexpressed in HeLa cells [41]. Thus, HeLa cells were chosen as the model to investigate the intracellular operation of this enzyme-free DNA circuit (Fig. 3A). We first evaluated the biostability of DNA circuit using PAGE, which is a fundamental feature of biomaterials for *in vivo* applications. As shown in Fig. 3B, after the DNA circuit is triggered by miR-21 with a ratio of 1:1, nearly no degradation is observed when the products are incubated with cell lysate even for 4 h. In contrast, the naked siRNAs are gradually degraded with prolong of time, suggesting that the DNA hairpins can well protect the siRNA sequences from degradation in complex physiological environment. Then, the colocalization experiments were carried out by staining cell nucleus with Hoechst 33342 to locate the distribution of miR-21 in HeLa cells. The green fluorescence of FAM can be readily observed at the nuclear periphery, illustrating the distribution of miR-21 in the cytoplasm which initiates the DNA circuit and results in the recovered fluorescence (Fig. 3C). To further demonstrate the feasibility of the proposed method in living cells, the HeLa cells were transfected with DNA circuit and R-circuit, respectively. After incubated for 4 h, the fluorescence can be easily observed in DNA circuit treated cells. However, since the intracellular miR-21 cannot initiate the assembly among hairpins with R-circuit, almost no fluorescence is generated. In addition, the HeLa cells pretreated with antisense miR-21 also show an extremely weak fluorescence after transfected with DNA circuit (Fig. 3D). These results indicate the successful operation of this enzyme-free DNA circuit in living cells, and the fluorescence signals are indeed produced triggered by miR-21.

To demonstrate the expression level of miR-21 in different cells, HeLa cells (human cervix carcinoma cell line), HepG2 cells (human liver cancer cell line) and L-02 cells (human normal liver cell line) are treated

with the DNA circuit, respectively (Fig. 4A). It has been reported that the amount of miR-21 in HeLa and HepG2 cells is higher than that in L-02 cells [42]. Accordingly, an obvious fluorescence recovery is observed in HeLa and HepG2 cells, while nearly no fluorescence is appeared in L-02 cells. Also, flow cytometry assay was carried out to detect the fluorescence changes (Fig. 4B). Compared with L-02 cells, the HeLa cells and HepG2 cells treated with DNA circuit demonstrate the significantly enhanced fluorescence signals, which further confirm the practicability and reliability of the proposed DNA self-assembly strategy for *in situ* imaging of miRNA in living cells.

Gene silencing and *in vitro* anticancer efficacy

The studies have reported that VEGF is a critical regulator of tumor-induced angiogenesis, which facilitates tumor growth and survival [43, 44]. Thus, we chose VEGF as the target gene in this work to evaluate the gene silencing and anticancer efficacy via *in situ* generation of VEGF siRNA. To investigate the gene silencing efficacy, the HeLa cells were incubated with naked siRNA, DNA circuit, C-circuit, R-circuit, and Lipo for 48 h, respectively. The VEGF mRNA expression was analyzed by qRT-PCR (quantitative real-time polymerase chain reaction). As shown in Fig. 5A, the HeLa cells transfected with C-circuit, R-circuit and Lipo show little inhibition effect with the VEGF mRNA expression above 93.02%. Compared with the naked siRNA-treated cells (70.78%), the VEGF mRNA expression level in HeLa cells is significantly decreased after incubated with DNA circuit (51.06%). Further, the inhibitory effect of VEGF protein expression was studied by western blot assay (Fig. 5B). As expected, the expression level of VEGF protein in DNA circuit-treated HeLa cells (35.54%) is lower than that in the naked siRNA group (58.11%). These results confirm that the *in situ* generation of VEGF siRNA via miR-21 triggered DNA circuit can induce an efficient gene silencing and reduce the corresponding protein expression, which provide an excellent way to improve the specificity and efficiency of gene therapy.

Subsequently, the antitumor efficacy was evaluated using cell counting kit-8 (CCK-8) assay. After incubating HeLa cells with different concentrations of DNA circuit, the cell viability reveals a concentration-dependent decrease (Additional file 1: Fig. S1). When the concentration of DNA circuit is 200 nM, the cell viability decreased to 33.09%. To further evaluate the therapeutic efficiency of *in situ* siRNA assembly, the HeLa cells were transfected with different samples including naked siRNA, DNA circuit, C-circuit, R-circuit and Lipo, respectively. As shown in Fig. 5C, no significant loss of viability is observed in HeLa cells after treated with C-circuit, R-circuit and Lipo, indicating the high specificity of the proposed DNA circuit. Notably, the inhibition effect of DNA circuit on Hela cells (67.14%) is obviously higher than that of naked siRNA (50.89%) due to the improved delivery stability and high reaction efficiency of DNA circuit. Moreover, the therapeutic effect is examined via cell apoptosis assays using Annexin V-FITC apoptosis detection kit (Fig. 5D). The HeLa cells treated with DNA circuit shows the highest apoptotic rate (42.40%) compared with the cells treated with naked siRNA (30.30%), C-circuit (0.16%), R-circuit (0.14%) and Lipo (0.06%). These results further demonstrate the improved stability and therapeutic effect of VEGF siRNA that are *in situ* generated triggered by endogenous miR-21.

Owing to the high expression of miR-21 in HepG2 cells, we further chose HepG2 cells to investigate the applicability of this enzyme-free DNA circuit for gene therapy. After transfected HepG2 cells with 200 nM DNA circuit, the expression of VEGF mRNA and the corresponding protein are inhibited to 48.04% and 41.92%, respectively (Additional files 1: Fig. S2a and S2b), which also verifies the excellent performance siRNAs that are *in situ* generated for gene silencing. In addition, a significant decrease in cell viability (53.16%) and increase in apoptosis rate (46.02%) are observed (Additional files 1: Fig. S2c and S2d), indicating the proposed enzyme-free DNA circuit can be used as a general treatment method for various cancer types with excellent therapeutic effect.

***In vivo* tumor therapy**

The *in vivo* antitumor efficacy of DNA circuit was evaluated using HeLa xenograft tumors. The mice were randomly divided into five groups (four mice per group). When the tumor volume reached $\sim 75 \text{ mm}^3$, the mice in each group were respectively treated with PBS, naked siRNA, DNA circuit, C-circuit and R-circuit via intratumor injection every other day for eight times, in which the dosage of siRNA was 0.25 mg/kg. The time schedule for treatment of tumor-bearing mice is shown in Fig. 6A. The variations of body weights in mice were monitored every 2 days during the treatment to evaluate the side effect of DNA circuit. From Fig. 6B, there is no obvious difference of body weight among the groups, demonstrating that the proposed DNA circuit has no significant side effect on the treated mice. During the treatment, the tumor volumes were measured to observe the tumor growth inhibition of the DNA circuit (Fig. 6C). For PBS, R-circuit and C-circuit treated groups, the tumor sizes increase rapidly, showing little inhibition on tumor growth in these cases, while the naked siRNA treated group reveals a weak inhibitory effect. Remarkably, the DNA circuit treated group exhibits the strongest antitumor effect. The photographs of mice under different treatments after 15 days are recorded (Additional files 1: Fig. S3), and the corresponding photos and the average weight of the removed tumors in different groups are shown in Fig. 6D and Fig. 6E, respectively. Furthermore, to test the antitumor effect of DNA circuit, the tumor tissues were analyzed with H&E staining and TUNEL assay (Fig. 6F). As expected, the tissue slices from DNA circuit group shows the most significant cell apoptosis and necrosis, demonstrating the excellent antitumor effect via *in situ* generation of siRNA.

Additionally, the pathological results of major organs (heart, liver, spleen, lung and kidney) were obtained by H&E staining (Fig. 7). All images exhibit the well-defined cytoplasm and nuclei, which has no noticeable abnormality compared with the PBS treated group, demonstrating the negligible side effects of DNA circuit *in vivo*. Therefore, the *in situ* generation of VEGF siRNA triggered by endogenous miR-21 provides a promising approach with the advantages of good biosafety and biocompatibility for highly efficient gene therapy of cervical carcinoma.

Conclusions

In summary, we have proposed an endogenous miR-21-responsive enzyme-free DNA circuit for *in situ* generation of VEGF siRNA and efficient gene therapy of cervical carcinoma. The proposed DNA self-

assembly protocol has demonstrated several unique advantages. (1) Easy operation. This strategy involves only three DNA hairpins, which can be specifically triggered by intracellular miR-21 for the formation of “DNWs” via isothermal strand displacement reaction without complicated design in sequences and the assistance of exogenous enzymes. (2) Multifunctionality. Through rational design, this work has readily realized sensitive diagnosis of cervical carcinoma upon recognized by miR-21. More importantly, the *in situ* generation of siRNA demonstrate better gene therapy efficiency than that of naked siRNA due to the increased stability of siRNA protected by DNA hairpin structures and the high reaction efficiency of DNA circuit. (3) Universality. This method can be easily extended to monitor any miRNA and *in situ* self-assembly of other siRNA by just changing the corresponding hairpin sequences. Overall, our proposed enzyme-free DNA circuit provides a new insight into the construction of multifunctional DNA nanomaterials, which holds great potential in nanotheranostics as well as precision and personalized medicine.

Abbreviations

DNWs: DNA nanowheels; FRET: fluorescence resonance energy transfer; VEGF: vascular endothelial growth factor; PCR: polymerase chain reaction; RCA: rolling circle amplification; FBS: Fetal bovine serum; DMEM: Dulbecco’s modified Eagle’s; TEMED: N, N, N', N'-tetramethyl ethylenediamine; PS: protect strand; AFM: Atomic Force Microscopy; SIBS: Shanghai Institutes for Biological Sciences; CLSM: Confocal laser scanning microscopy; SDS-PAGE: sodium dodecyl sulfate-polyacrylamide gel electrophoresis; PVDF: electro-transferred to polyvinylidene fluoride; H&E: hematoxylin and eosin; TUNEL: terminal deoxynucleotidyl transferase-mediated dUTP nick-end labeling; HeLa cells: human cervix carcinoma cell line; HepG2 cells: human liver cancer cell line; L-02 cells: human normal liver cell line; qRT-PCR: quantitative real-time polymerase chain reaction; CCK-8: cell counting kit-8.

Declarations

Acknowledgements

Not applicable.

Authors' contributions

SB and ZC conceived and supervised this project and revised the manuscript. QJ, KY and SY performed the experiments. QJ and SY analyzed the data and wrote the manuscript. TT, JZ and HC assisted with data analysis. All authors read and approved the final manuscript.

Funding

The authors greatly appreciate the support from the National Natural Science Foundation of China (22076087 and 81802923), the Special Funds of the Taishan Scholar Program of Shandong Province (tsqn20161028), the National Natural Science Foundation of Shandong Province (ZR2020JQ08 and

ZR2019MH121), the Youth Innovation Technology Program of Shandong Province (2019KJC029), the Collaborative Innovation Program of Jinan (2018GXRC033), and the Open Project of Chemistry Department of Qingdao University of Science and Technology (QUSTHX201928).

Availability data and materials

All data and materials of this study can be obtained from the corresponding author upon request.

Ethics approval and consent to participate

All the experiments involved in the study were approved by the animal ethics committee of The Affiliated Hospital of Qingdao University.

Consent for publication

Not applicable.

Competing interests

The authors declare no competing interest.

Author details

¹Department of Obstetrics and Gynecology, The Affiliated Hospital of Qingdao University, Qingdao University, Qingdao, 266003, PR China. ²College of Chemistry and Chemical Engineering, Qingdao University, Qingdao, 266071, PR China.

References

1. Mannoor K, Liao J, Jiang F. Small nucleolar RNAs in cancer. *Biochim Biophys Acta Rev Cancer*. 2012; 1826: 121-128.
2. Mihailovic MK, Chen A, Gonzalez-Rivera JC, Contreras LM. Defective ribonucleoproteins, mistakes in RNA processing, and diseases. *Biochemistry*. 2017; 56: 1367-1382.
3. Fire A, Xu SQ, Montgomery MK, Kostas SA, Driver SE, Mello CC. Potent and specific genetic interference by double-stranded RNA in *Caenorhabditis elegans*. *Nature*. 1998; 391: 06-811.
4. Wang S, Liu X; Chen S, Liu Z, Zhang X, Liang XJ, Li L. Regulation of Ca²⁺ signaling for drug-resistant breast cancer therapy with mesoporous silica nanocapsule encapsulated doxorubicin/siRNA cocktail. *ACS Nano*. 2019; 13: 274-283.
5. Kang SH, Revuri V, Lee SJ, Cho S, Park IK, Cho KJ, Bae WK, Lee Yk. Oral siRNA delivery to treat colorectal liver metastases. *ACS Nano*. 2017; 11: 10417-10429.
6. Godinho BMDC, Ogier JR, Darcy R, O'Driscoll CM, Cryan JF. Self-assembling modified β-cyclodextrin nanoparticles as neuronal siRNA delivery vectors: focus on Huntington's disease. *Mol Pharm*. 2013;

10: 640-649.

7. Ledford H. Gene-silencing technology gets first drug approval after 20-year wait. *Nature*. 2018; 560: 291-292.
8. Fan J, Liu Y, Liu L, Huang Y, Li X, Huang W. A Multifunction lipid-based CRISPR-Cas13a genetic circuit delivery system for bladder cancer gene therapy. *ACS Synth Biol*. 2020; 9: 343-355.
9. Francia V, Schiffelers RM, Cullis PR, Witzigmann D. The biomolecular corona of lipid nanoparticles for gene therapy. *Bioconjug Chem*. 2020; 31: 2046-2059.
10. Dohmen C, Edinger D, Fröhlich T, Schreiner L, Lächelt U, Troiber C, Rädler J, Hadwiger P, Vornlocher HP, Wagner E. Nanosized multifunctional polyplexes for receptor-mediated siRNA delivery. *ACS Nano*. 2012; 6: 5198-5208.
11. Qi X, Liu X, Matiski L, Rodriguez Del Villar R, Yip T, Zhang F, Sokalingam S, Jiang S, Liu L, Yan H, Chang Y. RNA origami nanostructures for potent and safe anticancer immunotherapy. *ACS Nano*. 2020; 14: 4727-4740.
12. Lin Y, Huang Y, Yang Y, Jiang L, Xing C, Li J, Lu C, Yang H. Functional self-assembled DNA nanohydrogels for specific telomerase activity imaging and telomerase-activated antitumor gene therapy. *Anal Chem*. 2020; 92: 15179-15186.
13. Singh RP, Hidalgo T, Cazade PA, Darcy R, Cronin MF, Dorin I, O'Driscoll CM, Thompson D. Self-Assembled Cationic β -Cyclodextrin Nanostructures for siRNA Delivery. *Mol Pharm*. 2019; 16: 1358-1366.
14. Wu C, Han D, Chen T, Peng L, Zhu G, You M, Qiu L, Sefah K, Zhang X, Tan W. Building a multifunctional aptamer-based DNA nanoassembly for targeted cancer therapy. *J Am Chem Soc*. 2013; 135: 18664-18650.
15. Meng L, Ma W, Lin S, Shi S, Li Y, Lin Y. Tetrahedral DNA nanostructure-delivered DNAzyme for gene silencing to suppress cell growth. *ACS Appl Mater Interfaces*. 2019; 11: 6850-6857.
16. Dong Y, Yao C, Zhu Y, Yang L, Luo D, Yang D. DNA functional materials assembled from branched DNA: Design, Synthesis, and Applications. *Chem Rev*. 2020; 120: 9420-9481.
17. Novak S, Zhang J, Kentzinger E, Rücker U, Portale G, Jung N, Jonas U, Myung JS, Winkler RG, Gompper G, Dhont JKG, Stiakakis E. DNA Self-Assembly Mediated by Programmable Soft-Patchy Interactions. *ACS Nano*. 2020; 14: 13524-13535.
18. Hiratani M, Kawano R. DNA Logic Operation with Nanopore Decoding To Recognize MicroRNA Patterns in Small Cell Lung Cancer. *Anal Chem*. 2018; 90: 8531-8537.
19. Dang MN, Gomez Casas C, Day ES. Photoresponsive miR-34a/nanoshell conjugates enable light-triggered gene regulation to impair the function of triple-negative breast cancer cells. *Nano Lett*. 2021; 21: 68-76.
20. Zeng D, Wang Z, Meng Z, Wang P, San L, Wang W, Aldalbahi A, Li L, Shen J, Mi X. DNA tetrahedral nanostructure-based electrochemical miRNA biosensor for simultaneous detection of multiple miRNAs in pancreatic carcinoma. *ACS Appl Mater Interfaces*. 2017; 9: 24118-24125.

21. Wang GK, Zhu JQ, Zhang JT, Li Q, Li Y, He J, Qin YW, Jing Q. Circulating microRNA: a novel potential biomarker for early diagnosis of acute myocardial infarction in humans. *Eur Heart J.* 2010; 31: 659-666.
22. Dong H, Lei J, Ding L, Wen Y, Ju H, Zhang X. MicroRNA: function, detection, and bioanalysis. *Chem Rev.* 2013; 113: 6207-6233.
23. Li C, Wang Z, Wang L, Zhang C. Biosensors for epigenetic biomarkers detection: A review. *Biosens Bioelectron.* 2019; 144: 111695.
24. Choi YS, Edwards LO, DiBello A, Jose AM. Removing bias against short sequences enables northern blotting to better complement RNA-seq for the study of small RNAs. *Nucleic Acids Res.* 2017; 45: e87.
25. Tian H, Sun Y, Liu C, Duan X, Tang W, Li Z. Precise quantitation of microRNA in a single cell with droplet digital PCR based on ligation reaction. *Anal Chem.* 2016; 88: 11384-11389.
26. Yue S, Li Y, Qiao Z, Song W, Bi S. Rolling circle replication for biosensing, bioimaging, and biomedicine. *Trends Biotechnol.* 2021; 10.1016/j.tibtech.2021.02.007.
27. Wang TH, Peng Y, Zhang C, Wong PK, Ho CM. Single-molecule tracing on a fluidic microchip for quantitative detection of low-abundance nucleic acids. *J Am Chem Soc.* 2005; 127: 5354-5359.
28. Kilic T, Erdem A, Ozsoz M, Carrara S. microRNA biosensors: Opportunities and challenges among conventional and commercially available techniques. *Biosens Bioelectron.* 2017; 99: 525-546.
29. Wang H, Wang H, Willner I, Wang F. High-performance biosensing based on autonomous enzyme-free DNA circuits. *Top Curr Chem.* 2020; 378: 20.
30. Ouyang T, Liu Z, Han Z, Ge Q. MicroRNA Detection Specificity: Recent Advances and Future Perspective. *Anal Chem.* 2019; 91: 3179-3186.
31. Li C, Luo M, Wang J, Niu H, Shen Z, Wu ZS. Rigidified DNA Triangle-Protected Molecular Beacon from Endogenous Nuclease Digestion for Monitoring microRNA Expression in Living Cells. *ACS Sens.* 2020; 5: 2378-2387.
32. Yue S, Song X, Song W, Bi S. An enzyme-free molecular catalytic device: dynamically self-assembled DNA dendrimers for *in situ* imaging of microRNAs in live cells. *Chem Sci.* 2019; 10: 1651-1658.
33. Zhu Z, Wu R, Li B. Exploration of solid-state nanopores in characterizing reaction mixtures generated from a catalytic DNA assembly circuit. *Chem Sci.* 2019; 10: 1953-1961.
34. Cheng H, Li W, Duan S, Peng J, Liu J, Ma W, Wang H, He X, Wang K. Mesoporous Silica Containers and Programmed Catalytic Hairpin Assembly/Hybridization Chain Reaction Based Electrochemical Sensing Platform for MicroRNA Ultrasensitive Detection with Low Background. *Anal Chem.* 2019; 91: 10672-10678.
35. Zhang J, Zhang H, Ye S, Wang X, Ma L. Fluorescent-Raman Binary Star Ratio Probe for MicroRNA Detection and Imaging in Living Cells. *Anal Chem.* 2021; 93: 1466-1471.
36. Yue S, Zhao T, Qi H, Yan Y, Bi S. Cross-catalytic hairpin assembly-based exponential signal amplification for CRET assay with low background noise. *Biosens Bioelectron.* 2017; 94: 671-676.

37. Bi S, Yue S, Wu Q, Ye J. Triggered and catalyzed self-assembly of hyperbranched DNA structures for logic operations and homogeneous CRET biosensing of microRNA. *Chem Commun.* 2016; 52: 5455-5458.
38. Zhou W, Liang W, Li X, Chai Y, Yuan R, Xiang Y. MicroRNA-triggered, cascaded and catalytic self-assembly of functional “DNAzyme ferris wheel” nanostructures for highly sensitive colorimetric detection of cancer cells. *Nanoscale.* 2015; 7: 9055-9061.
39. Ma Y, Cai F, Li Y, Chen J, Han F, Lin W. A review of the application of nanoparticles in the diagnosis and treatment of chronic kidney disease. *Bioact Mater.* 2020; 5: 732-743.
40. Wang H, Xu S, Fan D, Geng X, Zhi G, Wu D, Shen H, Yang F, Zhou X, Wang X. Multifunctional microcapsules: A theranostic agent for US/MR/PAT multi-modality imaging and synergistic chemo-photothermal osteosarcoma therapy. *Bioact Mater.* 2021; 10.1016/j.bioactmat.2021.05.004.
41. Xue Q, Liu C, Li X, Dai L, Wang H. Label-Free Fluorescent DNA Dendrimers for microRNA Detection Based On Nonlinear Hybridization Chain Reaction-Mediated Multiple G-Quadruplex with Low Background Signal. *Bioconjug Chem.* 2018; 29: 1399-1405.
42. Liu J, Cui M, Zhou H, Yang W. DNAzyme Based Nanomachine for in Situ Detection of MicroRNA in Living Cells. *ACS Sens.* 2017; 2: 1847-1853.
43. Ferrara N, Gerber HP, Lecouter J. The biology of VEGF and its receptors. *Nat Med.* 2003; 9: 669-676.
44. Hoeben A, Landuyt B, Highley MS, Wildiers H, Van Oosterom AT, De Bruijn EA. Vascular Endothelial Growth Factor and Angiogenesis. 2004; 56: 549-580.

Figures

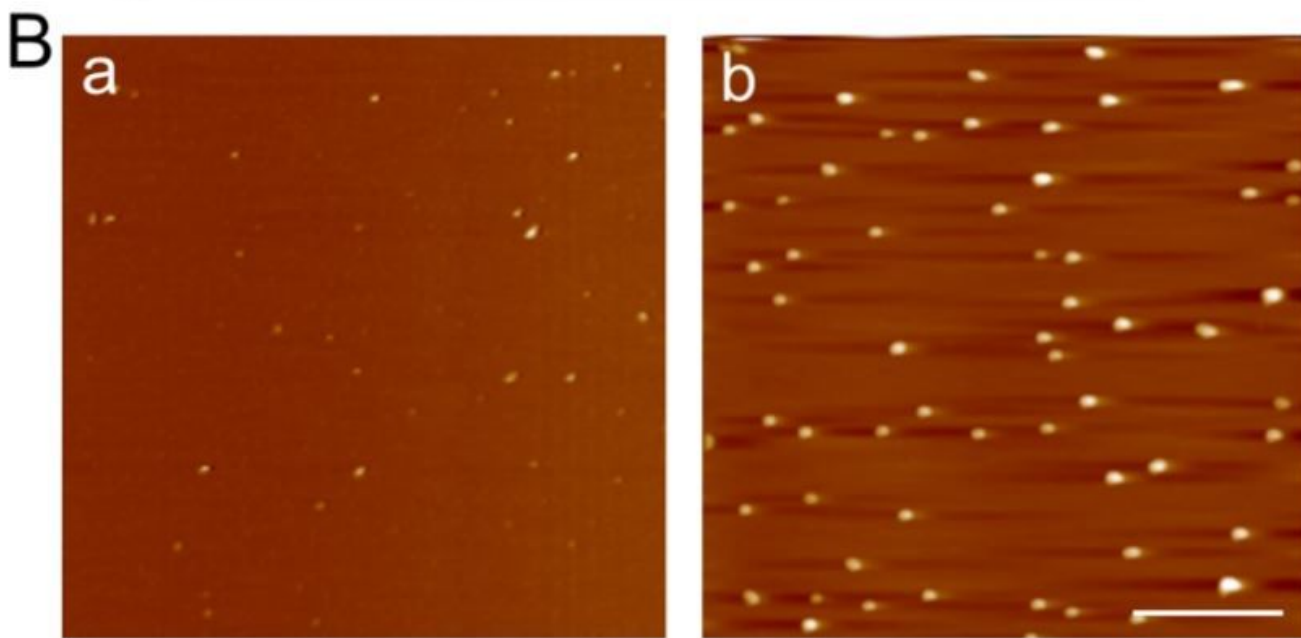
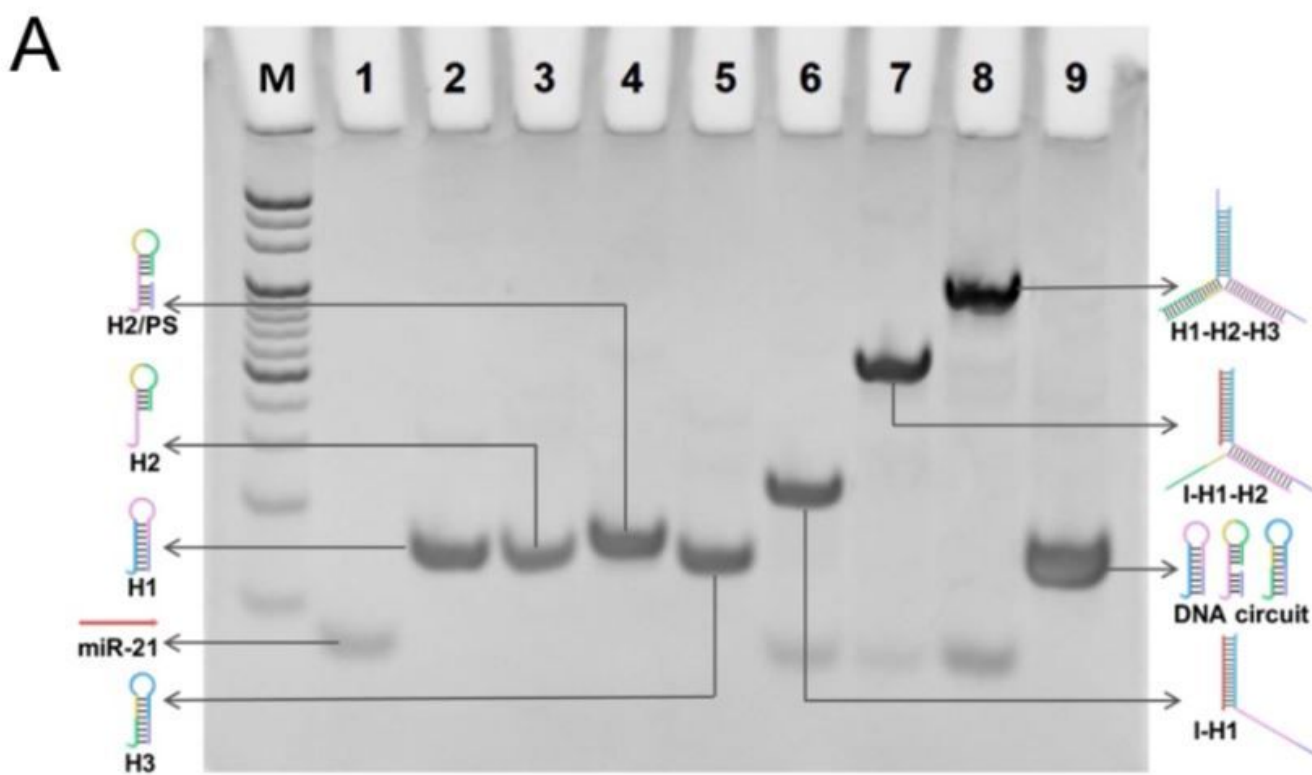


Figure 1

Characterization of the enzyme-free DNA circuit triggered by miR-21. (A) Native PAGE. Lane M: 20 bp DNA maker; Lane 1: miR-21; Lane 2: H1; Lane 3: H2; Lane 4: H2/PS; Lane 5: H3; Lane 6: miR-21 + H1; Lane 7: miR-21 + H1 + H2/PS; Lane 8: miR-21 + H1 + H2/PS + H3; Lane 9: H1 + H2/PS + H3 (control). The initial concentration of each hairpin is 10 μ M. (B) AFM images of DNA circuit (H1 + H2/PS + H3) (a) without and (b) with miR-21, respectively. Scale bar: 100 nm.

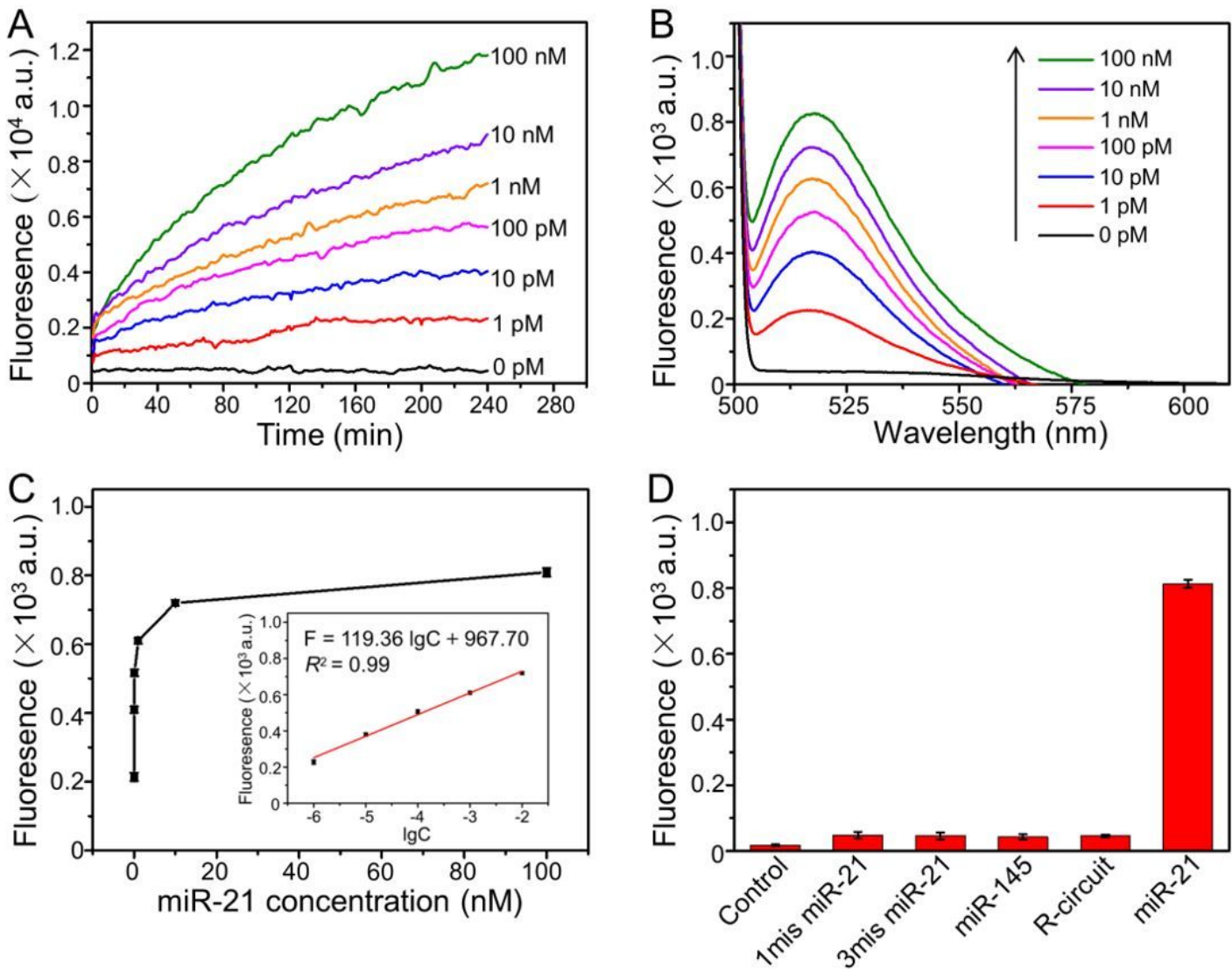


Figure 2

Sensitivity and selectivity of the enzyme-free DNA circuit triggered by miR-21. (A) Fluorescence kinetics of the DNA circuit triggered by various concentrations of miR-21 (from 1 pM to 100 nM). (B) The corresponding fluorescence spectra at 4 h. (C) Relationship of the fluorescence intensity at 520 nm to miR-21 concentration. Inset: the linear fit between the fluorescence intensity at 520 nm and the logarithmic value of miR-21 concentration. Error bars represent the standard deviation of three experiments. (D) Specificity of the DNA circuit in response to different analytes (final concentration is 100 nM).

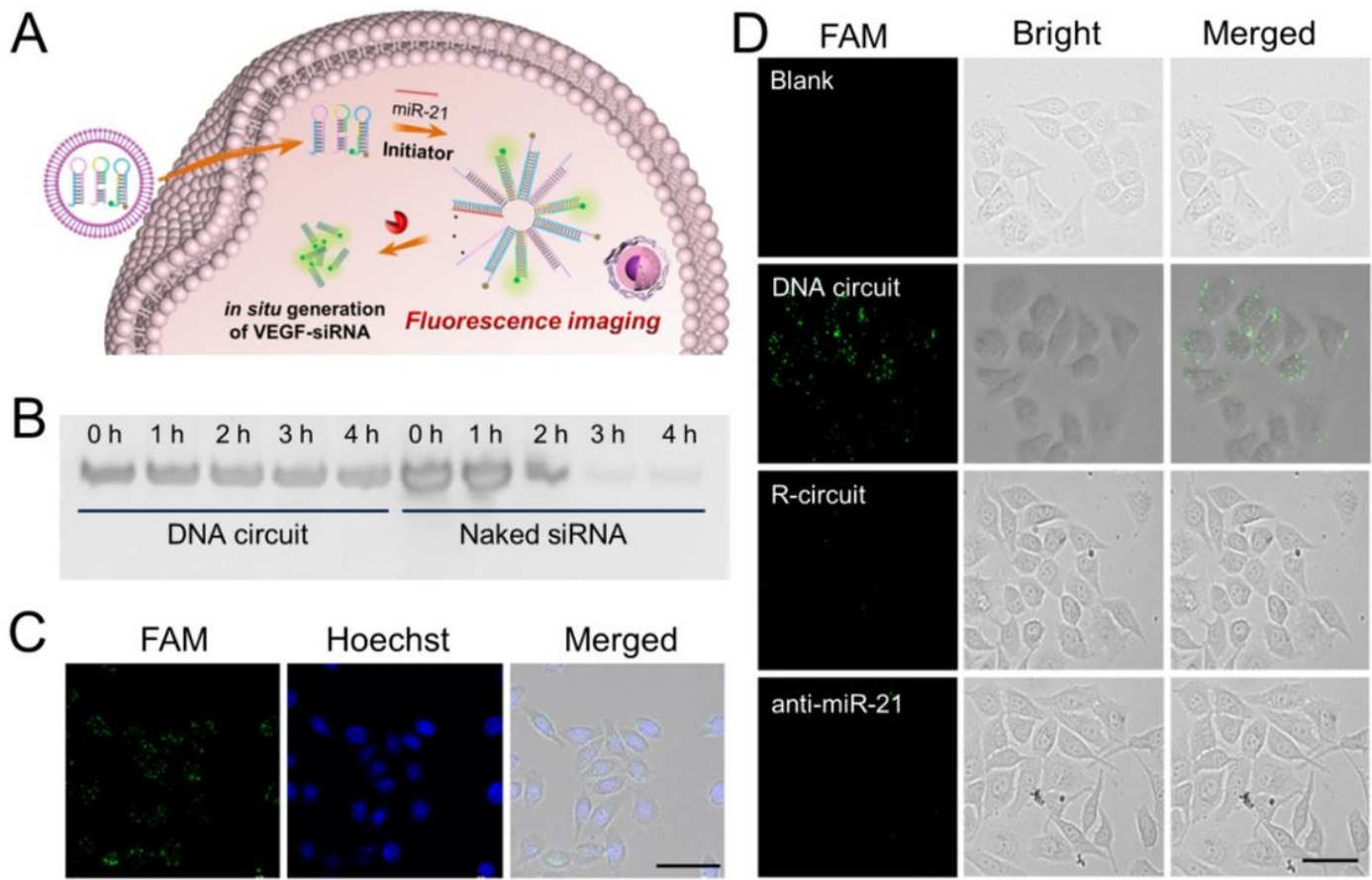


Figure 3

Visualization analysis of intracellular miR-21. (A) Schematics of *in situ* imaging of miR-21 in living cells. (B) Stability of DNA circuit and naked siRNA after incubation with cell lysate for 1 h, 2 h, 3 h and 4 h, respectively. (C) Nuclear localization images of HeLa cells after incubated with DNA circuit for 4 h. (D) CLSM images of HeLa cells with different treatments. The final concentration of each DNA hairpin is 200 nM. Scale bars in C and D: 50 μ m.

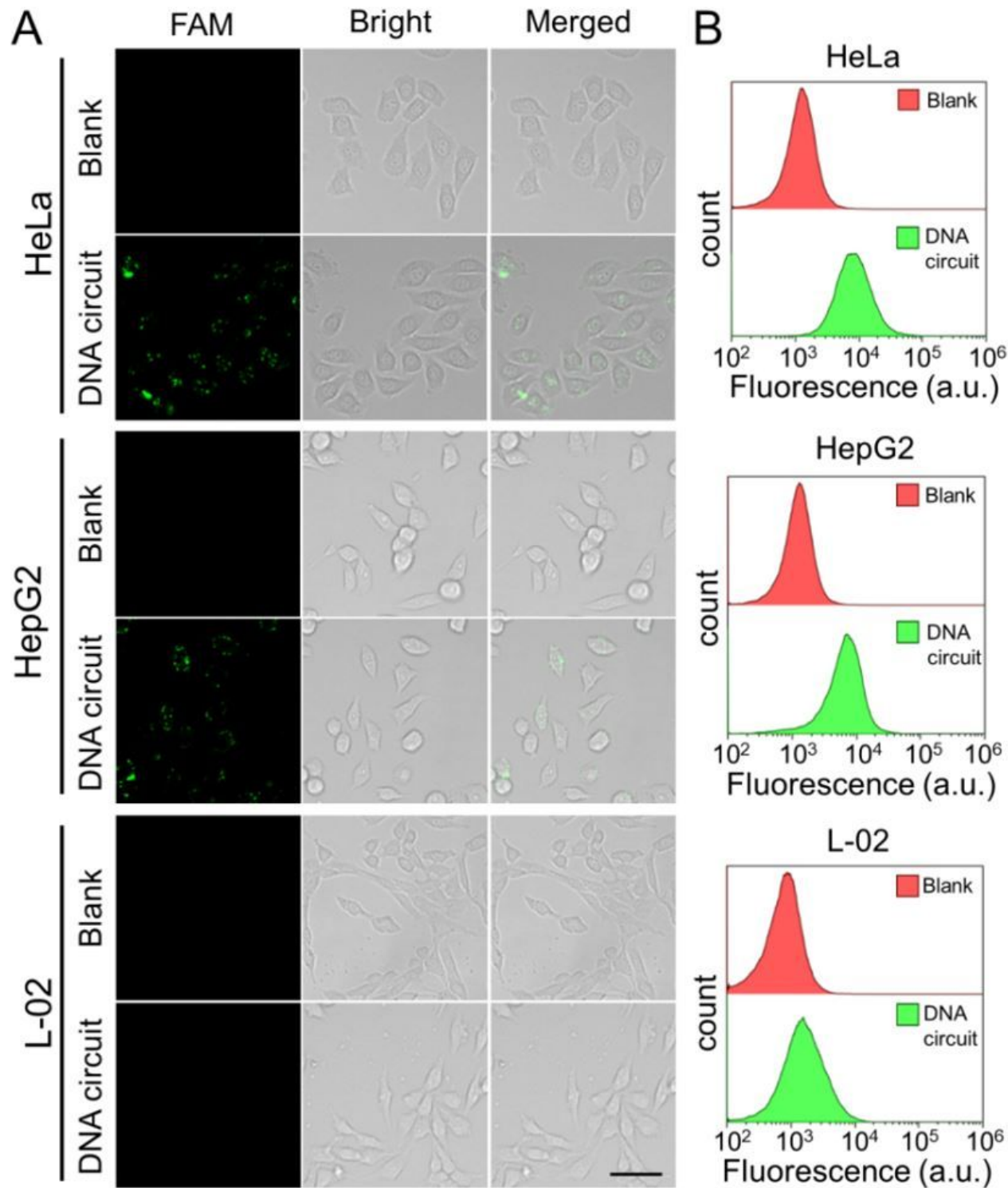


Figure 4

MiR-21 triggered enzyme-free DNA circuit in different cells. (A) CLSM images and (B) corresponding flow cytometric results of HeLa cells, HepG2 cells and L-02 cells after incubated with DNA circuit for 4 h. The final concentration of each DNA hairpin is 200 nM. Scale bar in A: 50 μ m.

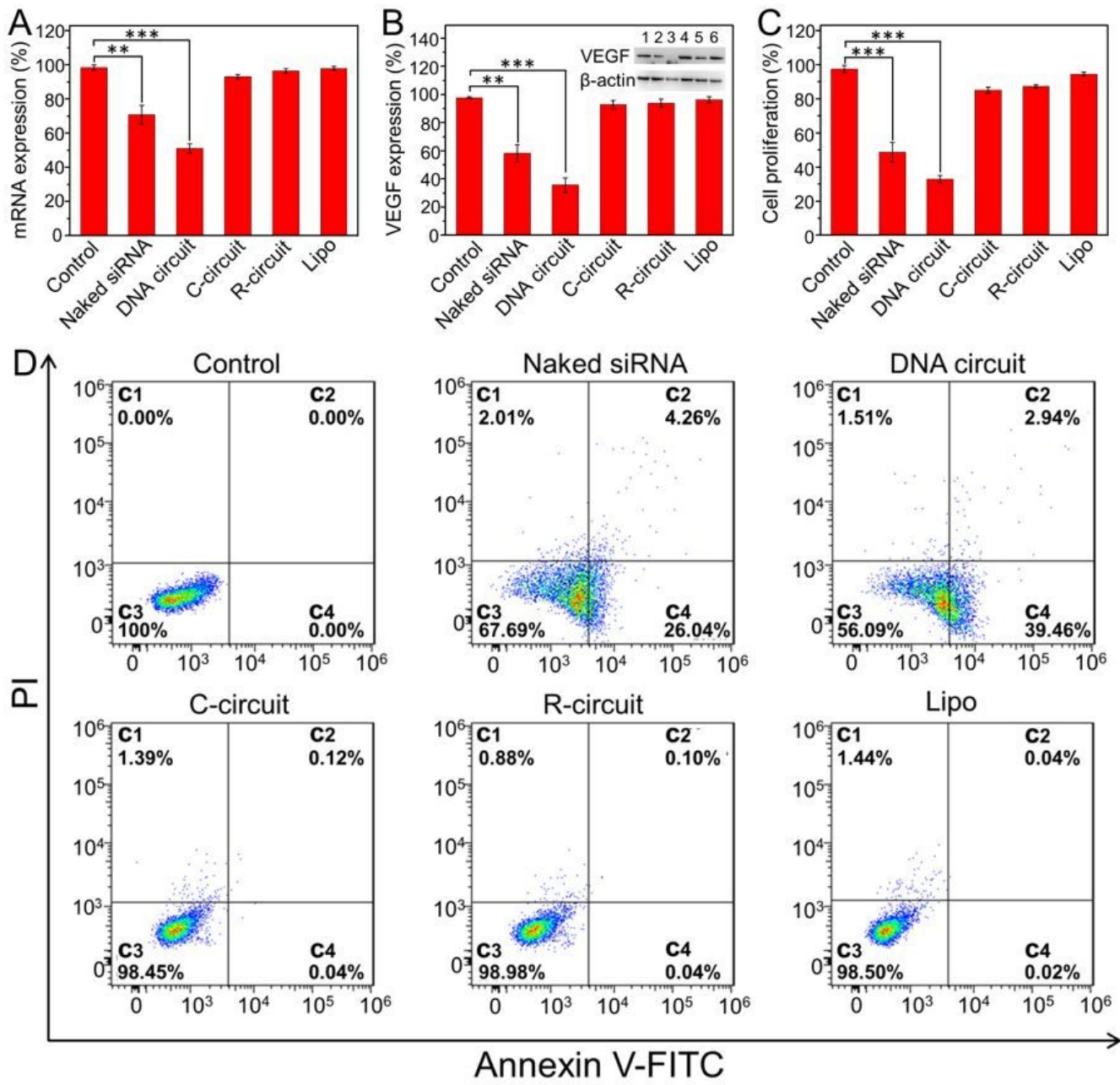


Figure 5

Intracellular therapeutic effect of the DNA circuit on HeLa cells. (A) VEGF mRNA expression, (B) VEGF protein expression, (C) proliferation and (D) apoptosis assays of HeLa cells after different treatments. Inset in B shows the western blot images. Lane 1: control; Lane 2: naked siRNA; Lane 3: DNA circuit; Lane 4: C-circuit; Lane 5: R-circuit; Lane 6: Lipo. The HeLa cells without any treatment are the control. The final concentration of each DNA hairpin is 200 nM. The data error bars indicate means \pm SD ($n = 3$). ** $P < 0.01$, *** $P < 0.001$ (two-tailed Student's t test).

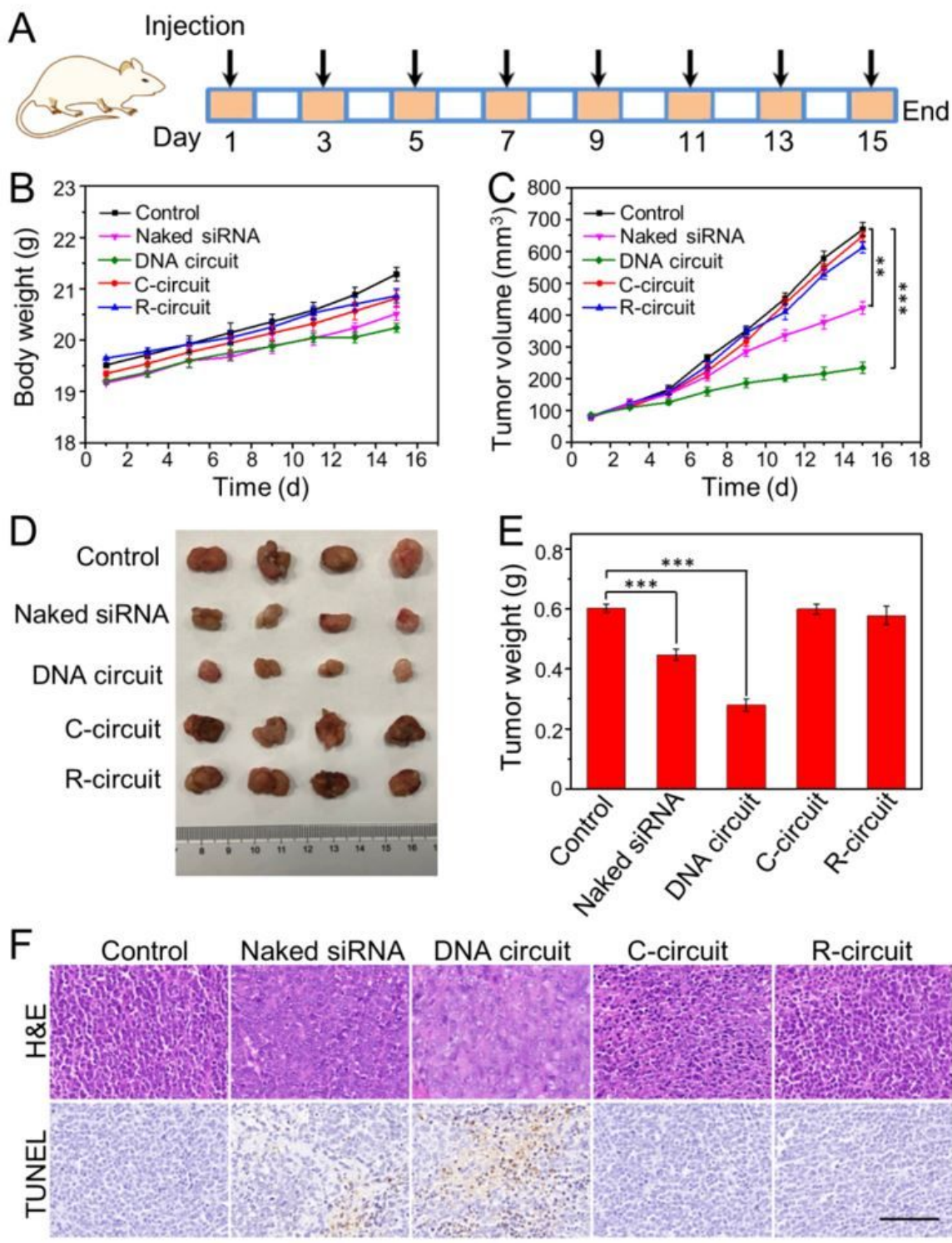


Figure 6

In vivo tumor therapy. (A) Time schedule for the treatment process. (B) Bodyweight and (C) tumor volume changes of mice in different groups during therapy. (D) Photographs of tumors dissected from HeLa tumor-bearing mice at the therapeutic terminal. (E) Tumor weight of mice in different groups after therapy. (F) H&E and TUNEL staining of tumor tissues with different treatments. Scale bar: 100 μ m. Error bars indicate means \pm SD ($n = 4$). ** $P < 0.01$, *** $P \leq 0.001$ (two-tailed Student's t test).

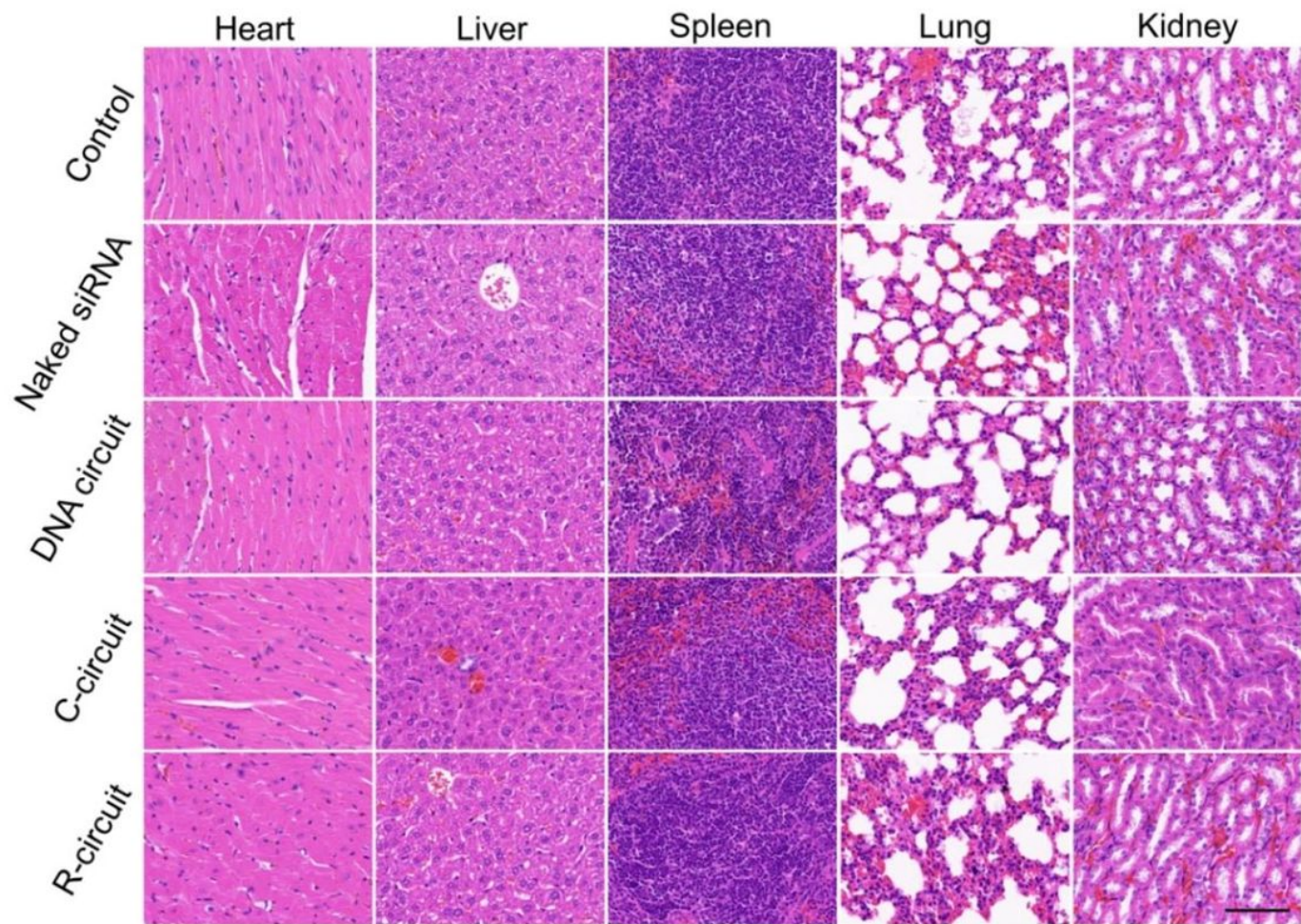


Figure 7

H&E staining of major organs (heart, liver, spleen, lung and kidney) from mice in different groups. Scale bar: 100 μm .

Supplementary Files

This is a list of supplementary files associated with this preprint. Click to download.

- [GraphicalAbstract.docx](#)
- [SupplementaryMaterial.docx](#)
- [scheme1.jpg](#)